Separable representation of the Paris nucleon-nucleon potential

J. Haidenbauer and W. Plessas
Institut für Theoretische Physik, Karl-Franzens-Universität Graz, A-8010 Graz, Austria
(Received 14 May 1984)

A separable representation of the Paris potential is constructed by means of the Ernst-Shakin-Thaler method. The resulting separable interactions represent a good approximation of the on-shell as well as off-shell properties of the Paris potential. Their form factors are composed of rational functions not too complicated for today's computer codes for few-body systems. The various features of the nucleon-nucleon force are discussed together with first results obtained with these separable potentials for elastic electron-deuteron and nucleon-deuteron scattering.

I. INTRODUCTION

The on-shell properties of the nucleon-nucleon (N-N) interaction can be considered as well established. This is due to the fact that both for the proton-proton (p-p) and the neutron-proton (n-p) systems we are given a large amount of reliable experimental data;[1,2] while they are rather accurate for p-p, they contain only minor uncertainties for n-p.[3] By assuming charge symmetry, which might be violated just slightly,[4] we can also get information on the neutron-neutron (n-n) system, since electromagnetic effects can be treated with satisfactory rigor in the transition from p-p to n-n observables.[5,6] As a consequence, realistic N-N interaction models all show similar on-shell properties despite the fact that they often result from different approaches to N-N dynamics.

However, the situation is not so obvious with respect to the off-shell behavior of the N-N interaction. The corresponding evidence can only be found in three- or more-particle problems involving an N-N subsystem.[7] Though there exist numerous investigations of N-N off-shell features from over the last decade or so, there is still much controversy and uncertainty about them.[8] In particular, it has been questioned which observables could provide constraints on the N-N off-shell behavior. From the theoretical side the situation has been much obscured by the use of N-N models often with unreasonable off-shell characteristics.[9] This is especially true for phenomenological separable potentials, which are still employed more than all other models and/or approaches. Separable representations of subsystem transition matrices constitute an essential tool for solving more refined three- or four-body problems; often, only by their use can numerical computations be facilitated such that more involved investigations become feasible. In the past, however, the N-N physics behind them was hardly realistic. As a consequence conclusions drawn from calculations with separable input were unreliable and sometimes even misleading.

In the past few years it became clear how important it was to include into the N-N subsystem specific features related to the (half-) off-shell behavior of the interaction. Above all this concerned the deuteron wave function in applications like e-d, π-d scattering[10–12] or ^{3}H and ^{3}He form factors.[13] Amongst the separable potentials providing a reasonable overall description of N-N on-shell data it was only the Graz-II model[6,14] that paid some attention to this aspect. But also off-shell properties from the N-N scattering domain were found to play a significant role evident, e.g., in polarized three-nucleon scattering processes.[15,16] In addition, recent studies of the inclusion of three-nucleon forces emphasized the need for a realistic off-shell behavior such as provided by meson-exchange potentials.[17]

In order to remedy the unpleasant situation with respect to a separable parametrization of the N-N interaction, we constructed a separable representation of the Paris potential[18] aiming at a reproduction both of its on-shell and off-shell characteristics. Thereby it should become possible to introduce all essential features of the N-N interaction (as resulting from meson-exchange dynamics) into few-particle calculations relying on well-approved integral equation approaches. As will be explained in Sec. II we made use of the Ernst-Shakin-Thaler (EST) separable approximation method[19] and adopted the Paris potential as the given N-N interaction model; it provides a realistic description of the N-N force, since it is basically derived from meson-exchange theory (see a more detailed description in the beginning of Sec. III) and shows a good fit to the modern N-N data base. Therefore it is very desirable to investigate in detail its (on-shell and off-shell) properties in few-body systems.

In Sec. II we give a short outline of the formalism necessary to apply the EST method. Thereafter we present the explicit forms of our separable representations of the Paris potential and discuss their on-shell and off-shell properties. Finally we also report on a first application of these separable interactions in three-nucleon scattering and mention a few preliminary results obtained for the triton binding energy.

II. SEPARABLE REPRESENTATION METHOD

In our examination of various separable approximation schemes we found the EST method[19] as the most direct and effective one to transpose on-shell as well as off-shell properties of a given two-body interaction into separable form.[20] In the literature there already exist some applications of this method to the N-N interaction,[21,22] but they

concern interaction models either unrealistic or out of date; furthermore, improper treatment of the method led to erroneous results as was pointed out by Haidenbauer and Plessas.[23]

Let us begin by considering the Lippmann-Schwinger equation for the radial wave function in the case of a general (spin-dependent) N-N interaction potential in some coupled partial-wave state of total angular momentum $J=l_<+1=l_>-1$:

$$|\psi^{(s)}_{EiL}\rangle = |\phi_{EL}\rangle\delta_{iL} + \sum_{L'=l_<,l_>} G^P_{0,L}(E)V_{LL'}|\psi^{(s)}_{EiL'}\rangle\ , \qquad (L=J\pm1) \quad (2.1)$$

with the incoming state $|\phi_{EL}\rangle$ of angular momentum $l=l_<$ or $l_>$. For this equation we have chosen standing-wave boundary conditions corresponding to the use of the principal-value Green's operator $G^P_{0,L}$. We remark, however, that the EST method to be outlined in the following works with other boundary conditions as well. We adopted this choice because it leads to simpler formulae and is easier to use in numerical computations.

The four equations (2.1) can be written in a more concise way by applying a matrix notation.[23] We combine the coupled wave functions $|\psi^{(s)}_{EiL}\rangle$ two by two into the kets $|\Psi^{(s)}_{Ei}\rangle$ representing two-dimensional column matrices. The potential and resolvent operators corresponding to this coupled partial-wave state with total angular momentum J become (2×2) matrices denoted by $\mathscr{V}$ and $\mathscr{G}^P_0$, respectively.

Given the potential $\mathscr{V}$—in our case it will be the Paris potential[18]—the EST method consists in constructing a rank-N separable potential $\tilde{\mathscr{V}}$ of the form

$$\tilde{\mathscr{V}} = \sum_{i,j=1}^{N} \mathscr{V}|\Psi_{\alpha_i}\rangle\lambda_{ij}\langle\Psi_{\alpha_j}|\mathscr{V}\ . \qquad (2.2)$$

Here the ensembles $\alpha_i=\{E_il_i\}$, $(i=1,\ldots,N)$, each denote a fixed energy E_i in some particular channel $l_i=l_<$ or $l_>$. The form factors of the separable potential $\tilde{\mathscr{V}}$ consist of the objects $\mathscr{V}|\Psi_{\alpha_i}\rangle$. Thus one can achieve the half-off-shell elements of the reaction (or equivalently transition) matrices $\tilde{R}_{Ll_i}(E_i)$ and $R_{Ll_i}(E_i)$ corresponding to $\tilde{\mathscr{V}}$ and $\mathscr{V}$, respectively, to be equal at the energies E_i of channel l_i by requiring

$$\sum_{j=1}^{N}\lambda_{ij}\langle\Psi_{\alpha_j}|\mathscr{V}|\Psi_{\alpha_k}\rangle=\delta_{ik}\ . \qquad (2.3)$$

This condition imposed on the potential strengths guarantees

$$\tilde{\mathscr{V}}|\Psi_{\alpha_i}\rangle=\mathscr{V}|\Psi_{\alpha_i}\rangle=\mathscr{R}(E_i)|\Phi_{\alpha_i}\rangle \qquad (2.4)$$

for N combinations α_i. This means that the on-shell as well as half-off-shell results for both interactions $\mathscr{V}$ and $\tilde{\mathscr{V}}$ are exactly the same at the energies E_i of channel l_i. At neighboring energies the separable potential $\tilde{\mathscr{V}}$ can be expected to provide a good approximation to the (half-) off-shell matrix $\mathscr{R}$ belonging to the original model $\mathscr{V}$. This approximation can be improved by selecting more and more interpolation energies E_i. We remark that E_i can also be chosen as a bound state energy; this will actually be the case in our treatment of the $^3S_1$-$^3D_1$ coupled channels (deuteron pole). The corresponding separable form factors are then furnished by the bound-state wave functions. Thus the EST method includes the possibilities offered by the unitary pole approximation (UPA).

The ensembles α_i have to be chosen according to the physical situation. In general, it turns out that for uncoupled partial waves of the N-N system it is sufficient to select two or three energies E_i in order to produce a good separable approximation to the original interaction over a wide energy domain, $E_{\rm lab}\lesssim500$ MeV, say. For coupled partial waves, notably the crucial $^3S_1$-$^3D_1$ state, at least four interpolation energies are needed.

However, also some care has to be taken in selecting the ensembles $\{E_il_i\}$. It is clear from Eq. (2.3) that the matrix $\langle\Psi_{\alpha_j}|\mathscr{V}|\Psi_{\alpha_k}\rangle$ must not become singular in the evaluation of the parameters λ_{ij}. Similarly one has to check carefully on the behavior of the matrix $(1-\Lambda\mathscr{G})$, with Λ containing the potential strengths λ_{ij} and $\mathscr{G}$ defined by the elements

$$G_{ij}(E)=\langle\Psi_{\alpha_i}|\mathscr{V}\mathscr{G}^P_0(E)\mathscr{V}|\Psi_{\alpha_j}\rangle\ . \qquad (2.5)$$

The matrix $(1-\Lambda\mathscr{G})$ enters into the denominator of the general solution for the reaction matrix $\tilde{\mathscr{R}}(E)$ pertaining to the separable interaction $\tilde{\mathscr{V}}$, namely,

$$\tilde{R}_{L'L''}(E',E'';E)=\langle\Phi_{E'L'}|\tilde{\mathscr{R}}(E)|\Phi_{E''L''}\rangle = \sum_{i,j=1}^{N}\langle\Phi_{E'L'}|\mathscr{V}|\Psi_{\alpha_i}\rangle D_{ij}(E) \times\langle\Psi_{\alpha_j}|\mathscr{V}|\Phi_{E''L''}\rangle \qquad (2.6)$$

for $L',L''=l_<,l_>$. The elements $D_{ij}(E)$ belong to the matrix

$$\mathscr{D}(E)=[\Lambda^{-1}-\mathscr{G}(E)]^{-1}=[1-\Lambda\mathscr{G}(E)]^{-1}\Lambda\ . \qquad (2.7)$$

Evidently the matrix $(1-\Lambda\mathscr{G})$ cannot become singular except at the location of a bound-state pole. In the construction of a separable potential via the EST method this fact has to be checked carefully. Otherwise it could lead to erroneous results like, e.g., in the case of Ref. 21, where an unphysical resonantlike behavior is produced in the scattering domain,[23] which was clearly not present in the model potential $\mathscr{V}$.

We note that the formalism given above reduces to uncoupled partial waves by setting $L=L'=l$. In this case the α_i need only be specified by the interpolation energies E_i (cf. also Ref. 23).

III. SEPARABLE APPROXIMATION TO THE PARIS POTENTIAL

We now discuss the application of the EST method to the case of the Paris potential. As already mentioned in the Introduction, the Paris model can be considered as a realistic description of the N-N force at least for internucleon separations $r\gtrsim0.8$ fm. There it represents meson-exchange dynamics—basically $(\pi+2\pi+\omega)$ exchange—

while in the interior ($r<0.8$ fm) it is parametrized phenomenologically. As a result it yields a good reproduction of the N-N on-shell data. But also the off-shell behavior—as far as relevant in nuclear physics processes—seems to be reasonable (we will come back to this aspect in Sec. IV). Above all it shows properties already found as essential in various three-particle reactions.[10–13,15–17] One is therefore eager to perform more detailed studies with this interaction. Since in its original version the Paris potential is of a very complicated form,[18] it has not yet been possible to employ it in the various few-particle problems aside from the particular 3-N bound-state case (e.g., in Refs. 24 and 25). By means of the separable parametrizations presented below it will become feasible to introduce all essential on-shell and off-shell characteristics of the Paris potential to these kind of problems; notably the particular separable forms will be well suited to existing computer codes based on integral-equation approaches.[26]

According to Eq. (2.2) the form factors of the separable potential $\tilde{\mathscr{V}}$ are furnished by the half-off-shell reaction matrices $\mathscr{R}(E_i)\,|\,\Phi_{\alpha_i}\rangle$ at the fixed energies E_i in some partial-wave state l_i. We obtained these objects by solving the Lippmann-Schwinger equation for the Paris potential. In order to guarantee an easy and good applicability of our potentials we cast these numerical form factors $\langle\Phi_{EL}\,|\,\mathscr{V}\,|\,\Psi_{\alpha_i}\rangle$ into rational functions of the type

$$g_{Li}(p)=\sum_{n=1}^{4}\frac{C_{Lin}p^{L+2(n-1)}}{(p^2+\beta_{Lin}^2)^{L+n}},\quad (L\le 1)$$
$$g_{Li}(p)=\sum_{n=1}^{4}\frac{C_{Lin}p^{L+2(n-1)}}{(p^2+\beta_{Lin}^2)^{L+n-1}},\quad (2\le L\le 3) \tag{3.1}$$
$$g_{Li}(p)=\sum_{n=1}^{4}\frac{C_{Lin}p^{L+2(n-1)}}{(p^2+\beta_{Lin}^2)^{L+n-2}},\quad (L\ge 4)$$

where $E=p^2\hbar^2/2\mu$. By adjusting the parameters C and β we could reproduce the numerical results (i.e., the half-off-shell functions $\langle\Phi_{EL}\,|\,\mathscr{V}\,|\,\Psi_{\alpha_i}\rangle$) up to $p\gtrsim 6$ fm^{-1} rather accurately. Above this region slight deviations occurred, but they were found to be negligible (cf. also the discussion of the off-shell behavior later on and Ref. 27). The potential strengths were then determined via

$$(\Lambda^{-1})_{ij}=g_{l_ij}(p_i)+\frac{2\mu}{\hbar^2}\sum_{L=l_<,l_>}P\int k^2dk\frac{g_{Li}(k)g_{Lj}(k)}{p_i^2-k^2},\quad (i\le j) \tag{3.2}$$

the "analytical" analog of

$$(\Lambda^{-1})_{ij}=\langle\Phi_{\alpha_i}\,|\,\mathscr{V}\,|\,\Psi_{\alpha_j}\rangle+\langle\Psi_{\alpha_i}\,|\,\mathscr{V}\mathscr{G}_0^P(E_i)\mathscr{V}\,|\,\Psi_{\alpha_j}\rangle \tag{3.3}$$

that follows from Eq. (2.3) with the use of Eq. (2.1). We denote the resulting potentials obtained in this way (namely, by representing the Paris potential in separable form by means of the EST method) by PESTN, where N specifies the rank of the separable interaction in each partial wave [cf. Eq. (2.2)]. Let us now discuss the partial-wave states provided by the Paris potential one after another.

A. Uncoupled partial waves

1. $^1S_0$

In this partial wave the Paris potential is given only for the p-p system.[18] In order to construct our separable approximation we first considered the purely nuclear case. We designed two different PEST potentials, one of rank 1

TABLE I. Interpolation energies selected for the construction of the separable potentials PESTN in various partial waves.

Partial wave	Abbreviation and rank	Selected energies E_i (MeV) or ensembles $\alpha_i=\{E_il_i\}$
$^1S_0$	PEST1	$E_1=0$
	PEST3	$E_1=0$ $E_2=100$ $E_3=300$
$^3P_0$	PEST2	$E_1=50$ $E_2=300$
$^1P_1$, $^3P_1$	PEST2	$E_1=50$ $E_2=150$
$^1D_2$, $^3D_2$		
$^3S_1$-$^3D_1$	PEST1	$\alpha_1=\{-2,2249,-\}$
	PEST4	$\alpha_1=\{-2,2249,-\}$ $\alpha_2=\{125,2\}$ $\alpha_3=\{100,0\}$ $\alpha_4=\{425,2\}$
$^3P_2$-$^3F_2$	PEST3	$\alpha_1=\{75,1\}$ $\alpha_2=\{175,3\}$ $\alpha_3=\{300,1\}$
$^3D_3$-$^3G_3$	PEST4	$\alpha_1=\{75,2\}$ $\alpha_2=\{200,4\}$ $\alpha_3=\{300,2\}$ $\alpha_4=\{400,4\}$

TABLE II. Parameters of the PESTN potentials in the $^1S_0$ partial wave. With respect to the n-p case, which is not contained in the original Paris potential, see the discussion in Sec. III A.

	p-p			n-p		
	β (fm^{-1})	C (fm^0)	λ (MeV fm^{-1})	β (fm^{-1})	C (fm^0)	λ (MeV fm^{-1})
PEST1	$\beta_{11}=1.111\,5753$	$C_{11}=-7.243\,9743$	$\lambda=-1.0$	$\beta_{11}=1.111\,5753$	$C_{11}=-7.315\,0006$	$\lambda=-1.0$
	$\beta_{12}=2.021\,232$	$C_{12}=-3.969\,7919$		$\beta_{12}=2.021\,232$	$C_{12}=-4.008\,7152$	
	$\beta_{13}=2.643\,4278$	$C_{13}=162.199\,14$		$\beta_{13}=2.643\,4278$	$C_{13}=163.789\,48$	
	$\beta_{14}=4.087\,7911$	$C_{14}=-360.465\,32$		$\beta_{14}=4.087\,7911$	$C_{14}=-363.999\,65$	
	$\beta_{11}=1.111\,5753$	$C_{11}=-572.2923$	$\lambda_{11}=-0.001\,021\,062$	$\beta_{11}=1.111\,5753$	$C_{11}=-773.800\,00$	$\lambda_{11}=-0.000\,5284$
	$\beta_{12}=2.021\,232$	$C_{12}=-313.6236$	$\lambda_{12}=0.022\,965\,747$	$\beta_{12}=2.021\,232$	$C_{12}=-424.052\,44$	$\lambda_{12}=0.015\,471\,054$
	$\beta_{13}=2.643\,4278$	$C_{13}=12\,814.143$	$\lambda_{13}=-0.013\,907\,568$	$\beta_{13}=2.643\,4278$	$C_{13}=17\,326.082$	$\lambda_{13}=-0.008\,800\,2556$
	$\beta_{14}=4.087\,7911$	$C_{14}=-28\,477.672$	$\lambda_{22}=-0.805\,816\,82$	$\beta_{14}=4.087\,7911$	$C_{14}=-38\,504.839$	$\lambda_{22}=-0.742\,248\,76$
	$\beta_{21}=1.029\,7944$	$C_{21}=-18.494\,719$	$\lambda_{23}=0.825\,8353$	$\beta_{21}=1.029\,7944$	$C_{21}=-18.494\,719$	$\lambda_{23}=0.770\,689\,24$
	$\beta_{22}=1.543\,5994$	$C_{22}=-53.628\,348$	$\lambda_{33}=-1.295\,7139$	$\beta_{22}=1.543\,5994$	$C_{22}=-53.628\,348$	$\lambda_{33}=-1.252\,8474$
PEST3	$\beta_{23}=2.612\,9194$	$C_{23}=925.424\,08$	$\lambda_{ij}=\lambda_{ji}$	$\beta_{23}=2.612\,9194$	$C_{23}=925.424\,08$	$\lambda_{ij}=\lambda_{ji}$
	$\beta_{24}=4.083\,7929$	$C_{24}=-2040.002$		$\beta_{24}=4.083\,7929$	$C_{24}=-2040.002$	
	$\beta_{31}=0.899\,518\,56$	$C_{31}=-2.883\,7445$		$\beta_{31}=0.899\,518\,56$	$C_{31}=-2.883\,7445$	
	$\beta_{32}=2.684\,3334$	$C_{32}=-84.344\,154$		$\beta_{32}=2.684\,3334$	$C_{32}=-84.344\,154$	
	$\beta_{33}=3.150\,5869$	$C_{33}=1163.1547$		$\beta_{33}=3.150\,5869$	$C_{33}=1163.1547$	
	$\beta_{34}=3.982\,6288$	$C_{34}=-2018.0523$		$\beta_{34}=3.982\,6288$	$C_{34}=-2018.0523$	

and one of rank 3, according to the interpolation energies specified in Table I. These two versions, whose parameters are given in Table II, reproduce the on-shell as well as half-off-shell properties of the Paris potential at threshold, since both contain $E_1=0$. In fact, the low-energy parameters of Paris and PESTN are the same for $^1S_0$ (p-p) purely nuclear (Table III); the small and unimportant discrepancy in r_s stems from the analytical approximation

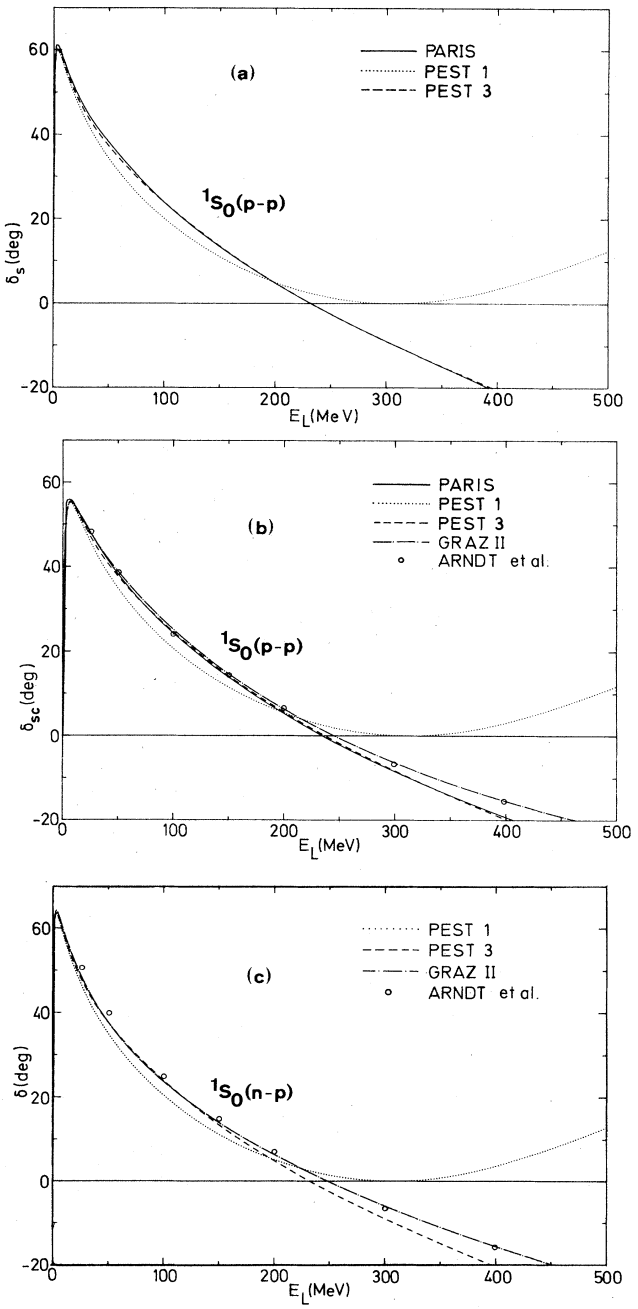

FIG. 1. $^1S_0$ phase shifts. (a) $^1S_0$ (p-p) purely nuclear phase shift δ_s. (b) $^1S_0$ (p-p) Coulomb-modified phase shift δ_{sc}. (c) $^1S_0$ (n-p). (b) and (c) also show a comparison to the latest Graz-II separable potential (Refs. 6 and 14) and to phenomenological data of Arndt *et al.* (Ref. 1).

TABLE III. Effective-range parameters in the $^1S_0$ state. The recalculated Paris results for $^1S_0$ (purely nuclear) differ slightly from what is quoted for $^1S_0$ (n-n) in the original work by the Paris group (Ref. 18). This is due to the different system of units we employ; we use an averaged reduced mass of $\mu = 469.463\,17$ MeV throughout.

	$^1S_0$ (p-p) Purely nuclear		$^1S_0$ (p-p) Coulomb modified		$^1S_0$ (n-p)	
	a_s (fm)	r_s (fm)	a_{sc} (fm)	r_{sc} (fm)	a (fm)	r (fm)
Paris	−17.54[a]	2.87[a]	−7.81[b]	2.80[b]		
PEST1	−17.54	2.86	−7.85	2.85	−23.72	2.81
PEST3	−17.54	2.86	−7.85	2.85	−23.72	2.81
Expt. (Ref. 28)			−7.8098±0.0023	2.767±0.010	−23.748±0.010	2.75±0.05

[a]Recalculated.
[b]Given by the authors (Ref. 18).

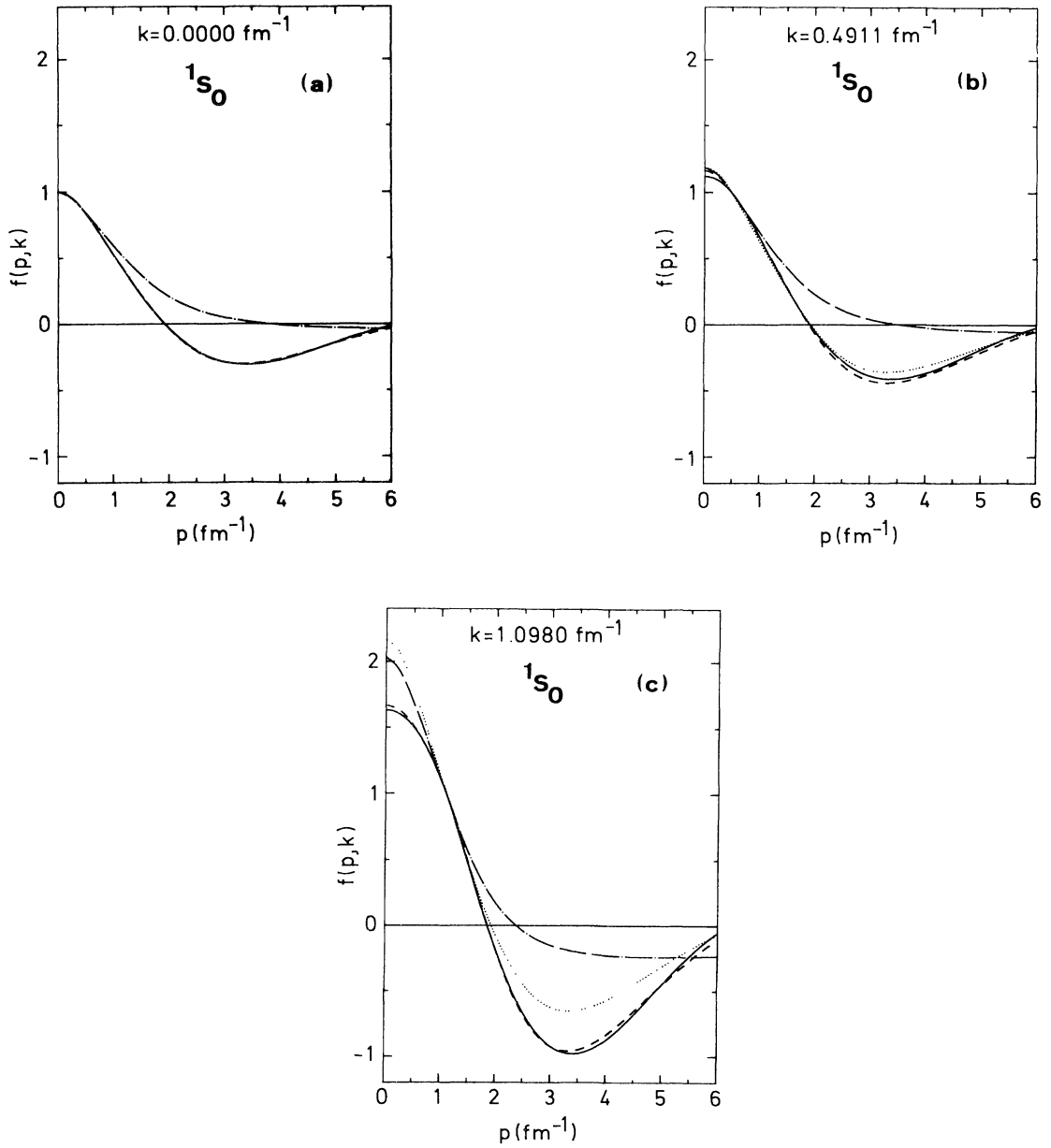

FIG. 2. Half-off-shell functions for $^1S_0$ (p-p) purely nuclear. (a) $E_{lab}=0$ MeV, (b) $E_{lab}=20$ MeV, (c) $E_{lab}=100$ MeV. In (a) PEST1 and PEST3 are identical. Same description as in Fig. 1.

of the numerical form factors. Also the corresponding phase shifts at low energies are the same for PESTN and Paris [Fig. 1(a)]. With increasing energy only PEST3 remains a good approximation.

Furthermore, the off-shell behavior at threshold is equivalent for PESTN and Paris. Figure 2(a) shows the Noyes-Kowalski half-off-shell functions

$$f(p,k)=\frac{R(p,k;k^2)}{R(k,k;k^2)} \tag{3.4}$$

at zero energy. Slight differences only occur for off-shell momenta $p>6$ fm^{-1}. They do not influence the reproduction of the on-shell data and are practically unimportant in three-body applications.[27,29] If we go to higher energies [Fig. 2(b) shows $f(p,k)$ at $E_{\rm lab}=20$ MeV] both the PEST1 and PEST3 approximations become slightly worse, but PEST3 improves again at $E_{\rm lab}=100$ MeV [Fig. 2(c)]. Note that in this case $E_2=100$ MeV was selected as the second interpolation energy (Table I). Moving further up with energy these properties recur for PEST3, since $E_3=300$ MeV was chosen. So in the case of PEST3 a rather accurate approximation is guaranteed up to $E_{\rm lab}\approx 500$ MeV.

Since three-particle calculations require as subsystem input the N-N amplitude for energies $-\infty<E\leq E_{3N}$ and off-shell momenta $0\leq p<\infty$ and $0\leq k<\infty$, we also checked on the reaction matrix elements $R(p,k;E)$ of PESTN and Paris at negative energies. These are shown in Figs. 3 and 4 for $E_{\rm lab}=0$ and -10 MeV, respectively. The figures look similar at other (positive or negative) energies, but the approximation eventually becomes less accurate for both p and k far off shell. In contrast to the half-off-shell behavior [for $E=0$ shown in Fig. 2(a)], the off-shell properties are slightly different for PEST1 and PEST3 even at the interpolation energy $E_1=0$, which was chosen for both cases. Formally the reason for this can be observed from the single-channel analog of Eq. (2.6). Both versions, however, still provide a reasonable approximation to the Paris potential even fully off shell.

Once the purely nuclear case is established, we can embed it into the long-range Coulomb field. The Coulomb distortion of the nuclear interaction for the p-p

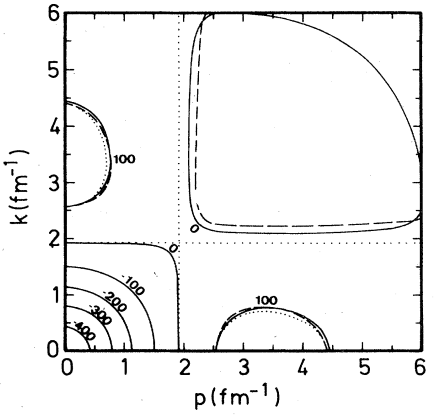

FIG. 3. $^1S_0$ purely nuclear off-shell reaction matrices $R(p,k;E)$ in units MeV fm^3 at $E=0$. Same description as in Fig. 1.

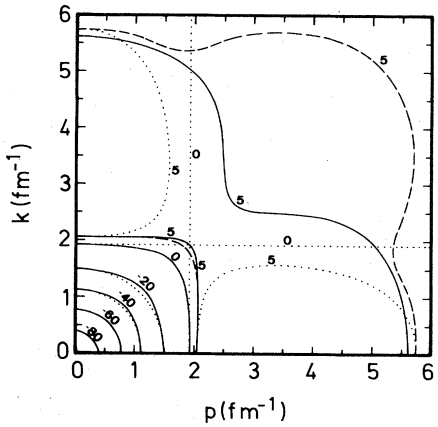

FIG. 4. Same as Fig. 3 at $E_{\rm lab}=-10$ MeV.

system can be treated rigorously both on shell and off shell via the formalism of Ref. 6. Especially the separable potential form factors of the type we chose in Eqs. (3.1) lend themselves to this kind of treatment. In particular, analytical formulae for Coulomb-modified on-shell as well as off-shell transition matrices (for all partial waves) can be deduced from the results already found in Ref. 6.

The Coulomb-modified effective-range parameters for the $^1S_0$ p-p system are given in Table III, while the pertinent phase shifts δ_{sc} are shown in Fig. 1(b) in comparison to the original Paris results and latest phenomenological data.[1] The latter are just quoted for the sake of interest. The Paris phases may fall apart from these data, because the Paris potential was fitted directly to the N-N scattering observables; furthermore, the data base in the analysis of Arndt *et al.*[1] is different from the one used by Lacombe *et al.*[18] Therefore the PEST potentials, as an approximation to the original Paris potential, should in the first place be judged by the Paris results. The comparison with the results of the separable Graz-II potential, which was constructed phenomenologically, should be interesting with respect to the (half-) off-shell behavior and the relative complexity of the two parametrizations.

For the Coulomb-modified p-p system the quality of the PEST approximations is typically the same as previously seen for the purely nuclear case. This is also true for the off-shell behavior; wherefore we abandon it to show these graphs.

For the $^1S_0$ state we finally consider the n-p system. Though the Paris potential does not contain this case, we provided PEST parametrizations also for $^1S_0$ (n-p), since various three-particle problems require a distinction between p-p and n-p in $^1S_0$. We obtained these potentials by simply shifting the Paris-type off-shell behavior, i.e., the purely nuclear p-p EST form factors, to the on-shell point that corresponds to n-p experimental data. This procedure, which in the main leaves the off-shell behavior unaltered, is justified by the observation that in meson-theoretical approaches to the N-N interaction there is practically no difference in the off-shell behavior between the p-p (purely nuclear) and the n-p system in the $^1S_0$ state.[30] The low-energy properties of our $^1S_0$ (n-p) PEST potentials are given in Table III together with a compar-

TABLE IV. Parameters of the PEST2 potentials in uncoupled P waves.

	β (fm^{-1})	C (fm^0)	λ (MeV fm^{-3})
		$^3P_0$	
	$\beta_{11}=1.869\,1379$	$C_{11}=-189.744\,07$	$\lambda_{11}=-0.146\,658\,88$
	$\beta_{12}=3.049\,9866$	$C_{12}=2096.7281$	$\lambda_{12}=0.405\,137\,83$
	$\beta_{13}=3.558\,5752$	$C_{13}=-3066.2694$	$\lambda_{22}=-5.478\,932$
	$\beta_{14}=1.159\,6292$	$C_{14}=102.753\,84$	$\lambda_{21}=\lambda_{12}$
PEST2			
	$\beta_{21}=2.551\,2467$	$C_{21}=59.861\,55$	
	$\beta_{22}=2.665\,1826$	$C_{22}=-681.320\,14$	
	$\beta_{23}=2.953\,7139$	$C_{23}=5265.5015$	
	$\beta_{24}=3.382\,713$	$C_{24}=-6825.757$	
		$^1P_1$	
	$\beta_{11}=1.622\,5099$	$C_{11}=76.181\,266$	$\lambda_{11}=0.669\,730\,64$
	$\beta_{12}=2.471\,2881$	$C_{12}=-381.785\,99$	$\lambda_{12}=-0.522\,031\,05$
	$\beta_{13}=2.712\,0059$	$C_{13}=1471.7803$	$\lambda_{22}=0.640\,755\,03$
	$\beta_{14}=3.164\,2803$	$C_{14}=-1646.4168$	$\lambda_{21}=\lambda_{12}$
PEST2			
	$\beta_{21}=1.769\,7160$	$C_{21}=61.335\,643$	
	$\beta_{22}=2.404\,9729$	$C_{22}=1348.5020$	
	$\beta_{23}=1.863\,1357$	$C_{23}=-842.102\,04$	
	$\beta_{24}=4.108\,4782$	$C_{24}=-1604.2632$	
		$^1P_1$	
	$\beta_{11}=1.565\,2079$	$C_{11}=89.398\,777$	$\lambda_{11}=0.445\,145\,49$
	$\beta_{12}=2.005\,8818$	$C_{12}=-208.135\,53$	$\lambda_{12}=-0.340\,6788$
	$\beta_{13}=2.410\,0051$	$C_{13}=425.344\,13$	$\lambda_{22}=0.445\,015\,14$
	$\beta_{14}=4.298\,1726$	$C_{14}=-630.352\,39$	$\lambda_{21}=\lambda_{12}$
PEST2			
	$\beta_{21}=1.546\,3024$	$C_{21}=43.477\,263$	
	$\beta_{22}=1.619\,6926$	$C_{22}=166.464\,66$	
	$\beta_{23}=2.000\,4143$	$C_{23}=-404.039\,68$	
	$\beta_{24}=2.179\,6197$	$C_{24}=528.135\,75$	

ison to experimental data.[28] Corresponding phase shifts are shown in Fig. 1(c). They are compared to n-p phenomenological phases[1] and to the Graz-II separable interaction.[14] The off-shell behavior is essentially of the type as shown in Figs. 2–4.

2. $^1P_1$, $^3P_{0,1}$

For each of these partial waves we constructed rank-2, PEST approximations. For the $^3P_{0,1}$ waves it was no longer necessary to distinguish between n-p and p-p except that for p-p the Coulomb-distortion effect had to be taken into account.[6] The interpolation energies were selected as quoted in Table I; the potential parameters are given in Table IV.

The on-shell properties of the PEST parametrization for $^3P_0$ are evident from the phase shift in Fig. 5. Up to $E_{\rm lab}\approx 70$ MeV the approximation to the Paris results is rather good, because $E_1=50$ MeV. Since the other interpolation energy had to be chosen as $E_2=300$ MeV to give due account to the high-energy repulsion, there is some discrepancy in the phase shifts around $E_{\rm lab}\approx 100$–150 MeV, but the situation improves again at higher energies. A better overall phase shift behavior would have required a rank-3 $^3P_0$ potential. Such a parametrization, however, would overcharge present three-particle codes and therefore we contented ourselves with rank 2.

The situation is easier with $^3P_1$ and $^1P_1$, because these phases are always negative. We aimed at an accurate

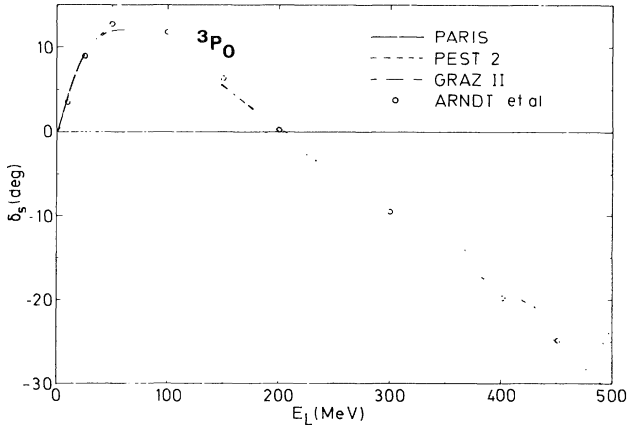

FIG. 5. $^3P_0$ purely nuclear phase shifts. The effect of the Coulomb distortion can be estimated from the figures given in Ref. 6 or Ref. 31.

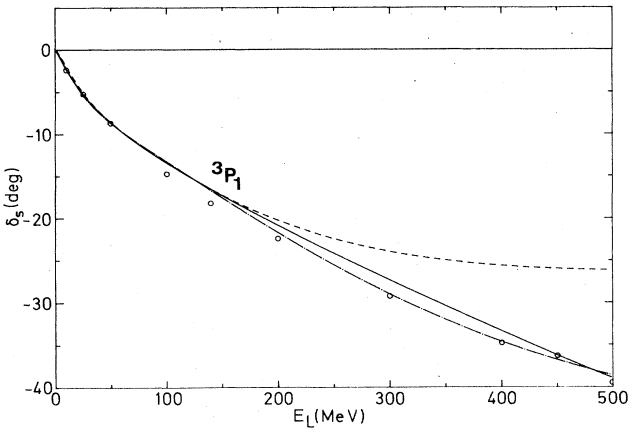

FIG. 6. $^3P_1$ purely nuclear phase shifts. Same description and remarks as for $^3P_0$ in Fig. 5.

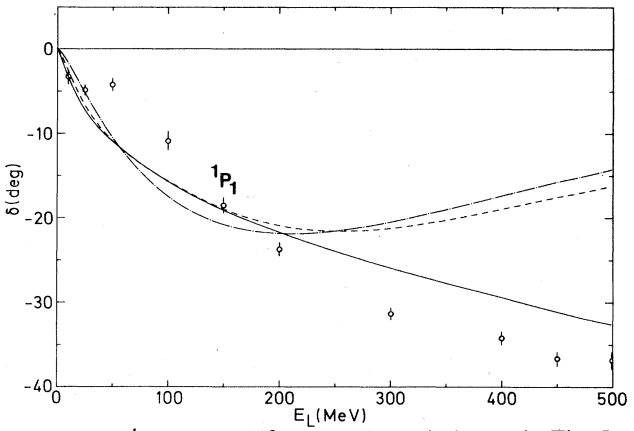

FIG. 7. $^1P_1$ phase shifts. Same description as in Fig. 5, except that the potential GRAZ-II is here substituted by GRAZ-I (Ref. 32).

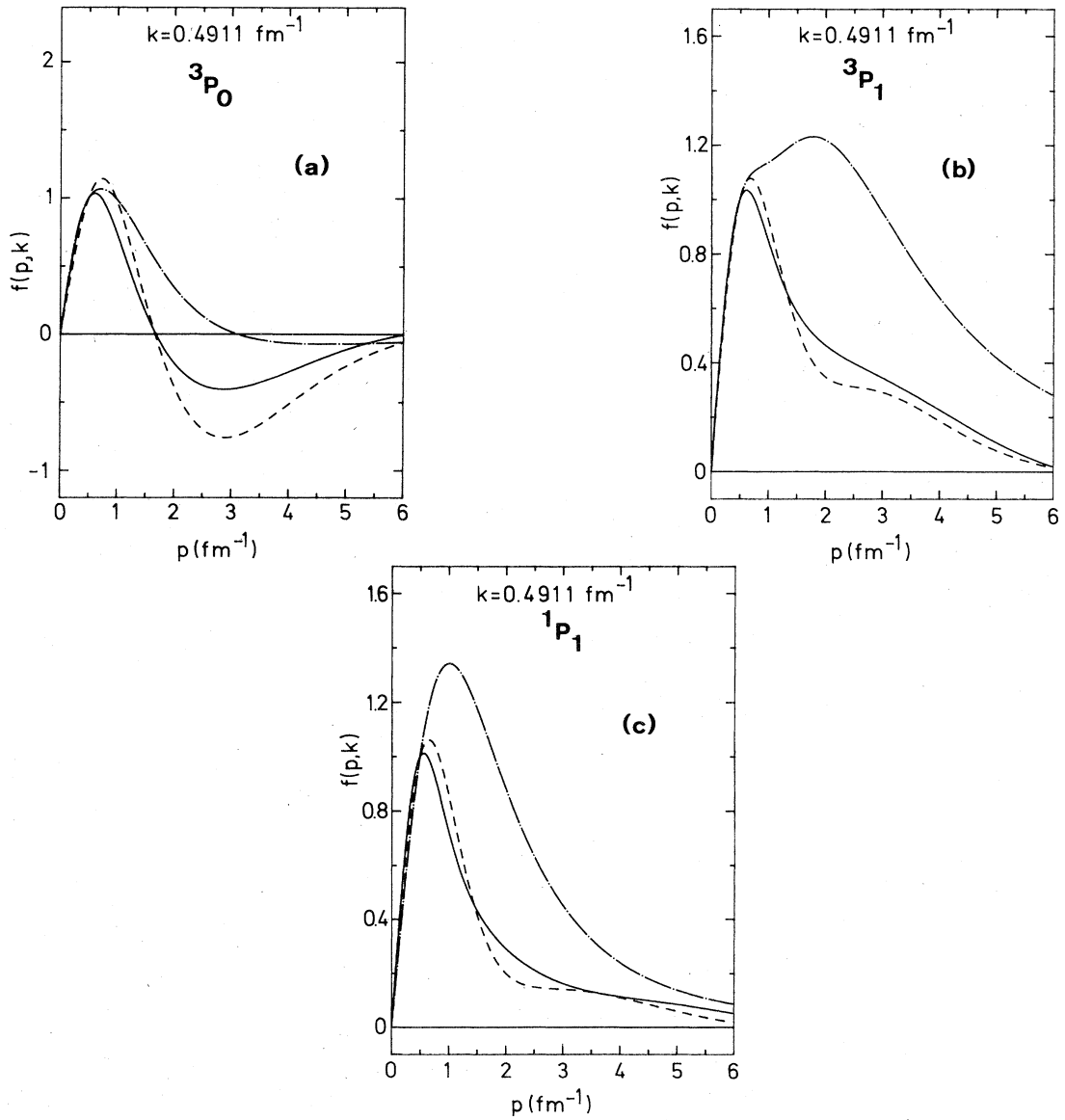

FIG. 8. Half-off-shell functions for uncoupled P waves at $E_{\rm lab}=20$ MeV. Same description as in Fig. 5. In (c) the dashed-dotted line belongs to GRAZ-I as in Fig. 7.

reproduction of the phase shifts predominantly at low and intermediate energies without exceeding rank 2 (Figs. 6 and 7). Thus for $E_{\text{lab}} \gtrsim 250$ MeV deviations from the original Paris results occurred. At first sight this seems surprising, since, e.g., the Graz-II potential[6] comes off with a better phase shift, particularly for $^3P_1$, with only rank 1. But one has to consider also the off-shell behavior. For traditional separable potentials and likewise for Graz-II it is grossly at variance with meson-theoretical predictions as shown by the Paris potential, say. The half-off-shell behavior of the PEST potentials, however, is a good approximation to the corresponding Paris potential properties; it is quite accurate at the two interpolation energies E_1 and E_2 and still reasonable elsewhere. As an example we show the half-off-shell functions at $E_{\text{lab}}=20$ MeV (Fig. 8), i.e., about halfway between threshold and E_1.

3. $^1D_2, ^3D_2$

For each of these partial waves we again constructed rank-2 PEST approximations. The properties of these potentials are practically the same as discussed above for the uncoupled P waves. The treatment of the Coulomb distortion for $^1D_2$ goes again along the lines of Ref. 6. The on-shell and off-shell behavior of the potentials, whose parameters are given in Table V, are shown in Figs. 9–11.

B. Coupled partial waves

1. $^3S_1 - ^3D_1$

This partial-wave state is crucial for a proper treatment of the N-N interaction. But up until now no satisfactory description of all its aspects has been achieved by means of separable forces. We tried to remedy this situation by constructing a rank-4 PEST approximation to the Paris potential. This separable interaction (parameters in Table VI) yields to a correct reproduction of the deuteron properties as well as to a fair description of the scattering domain up to $E_{\text{lab}} \approx 500$ MeV.

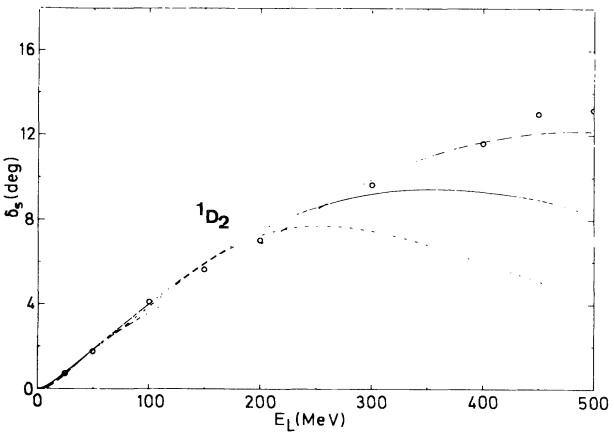

FIG. 9. $^1D_2$ purely nuclear phase shifts. Same description and remarks as in Fig. 5.

For certain applications, e.g., where just the deuteron bound state enters (like in elastic e-d scattering), we also provided a PEST1 parametrization assuming $E_1 = -E_D$. It is equivalent to a unitary-pole approximation to the Paris potential and is therefore unrealistic above threshold (see the discussion later in this section).

The location of the deuteron pole was selected as E_1 in both cases (Table I). Thereby it is guaranteed that all as-

TABLE V. Parameters of the PEST2 potentials in uncoupled D waves.

	β (fm^{-1})	C (fm^0)	λ (MeV fm^{-1})
		$^1D_2$	
	$\beta_{11}=1.169\,0501$	$C_{11}=-7.654\,1157$	$\lambda_{11}=-1.908\,6253$
	$\beta_{12}=1.335\,4235$	$C_{12}=3.839\,7789$	$\lambda_{12}=1.008\,5124$
	$\beta_{13}=3.631\,1131$	$C_{13}=-348.088\,99$	$\lambda_{22}=-0.975\,438\,27$
	$\beta_{14}=2.962\,3562$	$C_{14}=330.935\,49$	$\lambda_{21}=\lambda_{12}$
PEST2			
	$\beta_{21}=0.871\,579\,18$	$C_{21}=-1.086\,7868$	
	$\beta_{22}=1.285\,3211$	$C_{22}=-22.731\,322$	
	$\beta_{23}=3.245\,7085$	$C_{23}=265.302\,15$	
	$\beta_{24}=3.883\,9614$	$C_{24}=-303.609\,67$	
		$^3D_2$	
	$\beta_{11}=1.205\,5706$	$C_{11}=-40.322\,168$	$\lambda_{11}=-0.266\,741\,02$
	$\beta_{12}=1.296\,0008$	$C_{12}=-21.021\,097$	$\lambda_{12}=0.143\,051\,17$
	$\beta_{13}=1.623\,9653$	$C_{13}=533.480\,26$	$\lambda_{22}=-0.158\,172\,48$
	$\beta_{14}=1.445\,2618$	$C_{14}=-436.551\,62$	$\lambda_{21}=\lambda_{12}$
PEST2			
	$\beta_{21}=1.595\,3203$	$C_{21}=-245.060\,21$	
	$\beta_{22}=0.362\,699\,07$	$C_{22}=3.095\,0339$	
	$\beta_{23}=1.737\,0869$	$C_{23}=299.772\,37$	
	$\beta_{24}=0.587\,358\,27$	$C_{24}=42.826\,073$	

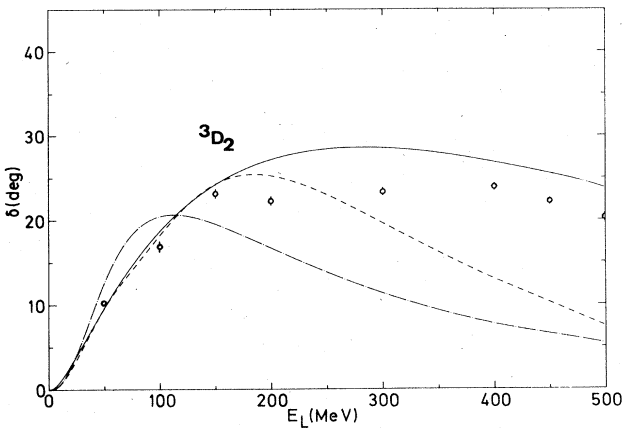

FIG. 10. $^3D_2$ phase shifts. Same description as in Fig. 5, except that the potential GRAZ-II is here substituted by GRAZ-I (Ref. 32).

pects of the deuteron (Table VII), including the wave functions (Fig. 12) of PEST1 as well as of PEST4, are practically the same as for the Paris potential; slight differences appear only for the wave functions, but in a domain relatively unimportant for nuclear problems. They stem from the analytical representation of the EST form factors (i.e., deuteron wave functions) by Eq. (3.1). These differences show up in the momentum-space wave functions at rather high momenta p (Fig. 12) corresponding to the very short-range region in configuration space ($r \lesssim 0.5$ fm). The properties, however, important in various few-particle problems, like e-d, π-d, N-d, e-^{3}He, and e-^{3}H scattering,[10–13] are taken into account adequately, i.e., the wave function behavior up to $p \approx 7$ fm^{-1} including especially the first zeros in $\psi_0(p)$ and $\psi_2(p)$. These latter features are of particular relevance, e.g., in polarized e-d scattering.[33]

At threshold both PEST1 and PEST4 are practically still equivalent to the Paris potential (see the effective-range parameters given also in Table VII). With increasing (positive) energy PEST1 becomes more and more unrealistic. This is because of the fact that a rank-1 separable potential cannot reproduce both the $^3S_1$ and $^3D_1$ phase shifts correctly. In this connection we remark that a PEST1 approximation to the $^3S_1$ state only (i.e., $^3S_1$ considered as uncoupled) was presented by Zankel *et al.*[16] As for $^1S_0$, also treated in that work, their PEST parametrization relies on form factors composed of rational functions different from the ones used in Eq. (3.1) for the present work; this parametrization is sometimes easier to handle, e.g., with regard to certain integrations, but involves more parameters.

The PEST4 parametrization is a close approximation to the Paris potential in the whole scattering domain up to $E_{\rm lab} \approx 500$ MeV (Figs. 13—15). In particular, the mixing parameter ϵ_1, which in earlier separable potentials could hardly be reproduced together with all other $^3S_1$-$^3D_1$ data (including an accurate deuteron), results reasonably, especially if compared to experimental data of Ref. 2, which are additionally given in Fig. 14.

The half-off-shell behavior in $^3S_1$-$^3D_1$ is exemplified in Fig. 16 for $E_{\rm lab} = 100$ MeV, i.e., both at and aside interpo-

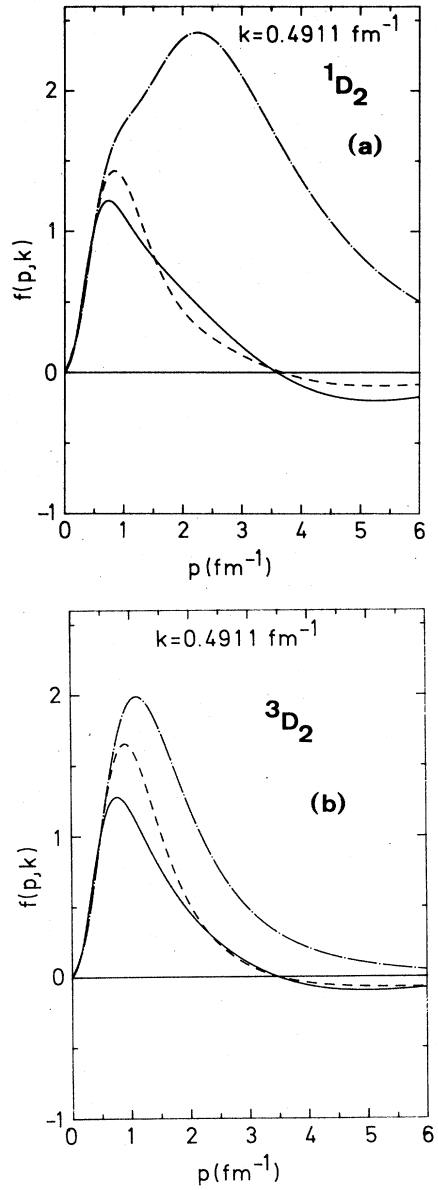

FIG. 11. Half-off-shell functions for uncoupled D waves at $E_{\rm lab} = 20$ MeV. Same description as in Fig. 5. In (b) the dashed-dotted line belongs to GRAZ-I as in Fig. 10.

lation energies (cf. Table I); a comparison is given again to Graz-II. It is evident that with PEST4 a good approximation of the characteristics of the Paris potential is achieved. Because of the balanced distribution of ensembles $\{E_i l_i\}$ these features are maintained over the whole energy range. We also observe that the behavior of Graz-II is grossly unrealistic [perhaps with the exception of the diagonal elements in Figs. 16(a) and (d)], like it is for most other conventional separable forces.[9]

2. $^3P_2$-$^3F_2$

In these coupled partial waves we again first dealt with the purely nuclear case. The Coulomb distortion was then introduced according to the formalism of Schweiger *et al.*

TABLE VI. Parameters of the PESTN potentials in the coupled $^3S_1$-$^3D_1$ partial-wave state.

	β (fm^{-1})	C (fm^0)	λ (MeV fm^{-1})	β (fm^{-1})	C (fm^0)
	$L=0$			$L=2$	
	$\beta_{11}=1.685\,5291$	$C_{11}=-17.392\,012$	$\lambda=-1.0$	$\beta_{11}=2.622\,8398$	$C_{11}=-139.845\,69$
	$\beta_{12}=3.920\,5339$	$C_{12}=260.914\,55$		$\beta_{12}=1.881\,5276$	$C_{12}=53.407\,791$
PEST1	$\beta_{13}=5.763\,6834$	$C_{13}=-1146.8056$		$\beta_{13}=3.834\,678$	$C_{13}=302.782\,58$
	$\beta_{14}=6.041\,9695$	$C_{14}=949.116\,89$		$\beta_{14}=4.995\,9386$	$C_{14}=-270.0781$
	$\beta_{11}=1.685\,5291$	$C_{11}=-51.009\,539$	$\lambda_{11}=-0.254\,222\,42$	$\beta_{11}=2.622\,8398$	$C_{11}=-410.157\,51$
	$\beta_{12}=3.920\,5339$	$C_{12}=765.2439$	$\lambda_{12}=-0.171\,787\,72$	$\beta_{12}=1.881\,5276$	$C_{12}=156.641\,27$
	$\beta_{13}=5.763\,684$	$C_{13}=-3363.4996$	$\lambda_{13}=0.071\,723\,814$	$\beta_{13}=3.834\,678$	$C_{13}=888.039\,85$
	$\beta_{14}=6.041\,9695$	$C_{14}=2783.6926$	$\lambda_{14}=0.005\,105\,0109$	$\beta_{14}=4.995\,9386$	$C_{14}=-792.119\,94$
	$\beta_{21}=1.787\,79$	$C_{21}=-68.041\,32$	$\lambda_{22}=0.087\,724\,39$	$\beta_{21}=1.909\,8545$	$C_{21}=87.065\,827$
	$\beta_{22}=2.175\,921$	$C_{22}=488.861\,19$	$\lambda_{23}=0.094\,518\,781$	$\beta_{22}=1.117\,0776$	$C_{22}=20.554\,605$
	$\beta_{23}=2.470\,5717$	$C_{23}=-1199.164$	$\lambda_{24}=-0.079\,244\,845$	$\beta_{23}=1.425\,9853$	$C_{23}=-65.702\,538$
	$\beta_{24}=2.730\,3931$	$C_{24}=871.796\,04$	$\lambda_{33}=-0.030\,645\,992$	$\beta_{24}=3.073\,4784$	$C_{24}=-91.839\,262$
PEST4	$\beta_{31}=1.597\,1102$	$C_{31}=-89.517\,302$	$\lambda_{34}=-0.034\,997\,609$	$\beta_{31}=2.643\,1889$	$C_{31}=143.6215$
	$\beta_{32}=9.967\,8931$	$C_{32}=2582.2164$	$\lambda_{44}=0.169\,553\,43$	$\beta_{32}=2.748\,3825$	$C_{32}=6.474\,4841$
	$\beta_{33}=4.594\,8011$	$C_{33}=-3042.3325$	$\lambda_{ij}=\lambda_{ji}$	$\beta_{33}=1.928\,3993$	$C_{33}=-1384.0981$
	$\beta_{34}=2.120\,6347$	$C_{34}=1235.3473$		$\beta_{34}=2.289\,1433$	$C_{34}=1550.1289$
	$\beta_{41}=4.026\,8195$	$C_{41}=-382.758\,56$		$\beta_{41}=4.259\,8369$	$C_{41}=366.501\,18$
	$\beta_{42}=5.046\,6356$	$C_{42}=1005.8091$		$\beta_{42}=2.146\,3834$	$C_{42}=263.872\,02$
	$\beta_{43}=2.579\,5951$	$C_{43}=2298.7534$		$\beta_{43}=2.490\,5282$	$C_{43}=-611.668\,11$
	$\beta_{44}=2.395\,3665$	$C_{44}=-2718.2533$		$\beta_{44}=2.293\,0841$	$C_{44}=-12.606\,207$

TABLE VII. Triplet effective-range parameters and deuteron properties.

	a_t (fm)	r_t (fm)	E_D (MeV)	Q_D (fm^2)	p_D (%)	η
Paris	5.43	1.77	2.2249	0.279	5.77	0.0261
PEST1	5.41	1.75	2.2249	0.279	5.77	0.0261
PEST4	5.41	1.76	2.2249	0.279	5.77	0.0261
Expt. (Refs. 28, 34, and 35)	5.424±0.004	1.759±0.005	2.2246±0.000 05	0.286±0.0015		0.0271±0.0004

TABLE VIII. Parameters of the PEST3 potential in the coupled $^3P_2$-$^3F_2$ partial-wave state.

	β (fm^{-1})	C (fm^0)	λ (MeV fm^{-3})	β (fm^{-1})	C (fm^0)
	$L=1$			$L=3$	
	$\beta_{11}=1.445\,2936$	$C_{11}=-28.609\,391$	$\lambda_{11}=0.046\,725\,027$	$\beta_{11}=1.166\,7491$	$C_{11}=0.967\,444\,07$
	$\beta_{12}=2.017\,3835$	$C_{12}=-186.150\,68$	$\lambda_{12}=0.417\,104\,84$	$\beta_{12}=1.540\,6619$	$C_{12}=166.309\,12$
	$\beta_{13}=5.446\,3467$	$C_{13}=-1094.0574$	$\lambda_{13}=-0.060\,922\,483$	$\beta_{13}=2.380\,2869$	$C_{13}=-119.421\,76$
	$\beta_{14}=2.849\,0316$	$C_{14}=1022.0712$	$\lambda_{22}=0.254\,924\,96$	$\beta_{14}=4.833\,5309$	$C_{14}=366.969\,81$
	$\beta_{21}=1.899\,3563$	$C_{21}=65.794\,074$	$\lambda_{23}=-0.414\,817\,03$	$\beta_{21}=1.095\,5323$	$C_{21}=-0.638\,684\,15$
	$\beta_{22}=2.454\,7294$	$C_{22}=173.01447$	$\lambda_{33}=-0.135\,935\,96$	$\beta_{22}=1.602\,0596$	$C_{22}=-37.538\,146$
PEST3	$\beta_{23}=1.549\,9793$	$C_{23}=-190.405\,69$	$\lambda_{ij}=\lambda_{ji}$	$\beta_{23}=4.458\,5234$	$C_{23}=-316.975\,99$
	$\beta_{24}=5.977\,3387$	$C_{24}=-217.747\,04$		$\beta_{24}=1.825\,4989$	$C_{24}=179.593\,23$
	$\beta_{31}=2.965\,9955$	$C_{31}=-327.4079$		$\beta_{31}=2.108\,4981$	$C_{31}=-47.364\,933$
	$\beta_{32}=4.932\,4835$	$C_{32}=-2950.6615$		$\beta_{32}=3.197\,7404$	$C_{32}=2035.5781$
	$\beta_{33}=2.905\,1889$	$C_{33}=4127.4473$		$\beta_{33}=3.957\,3349$	$C_{33}=-5925.4169$
	$\beta_{34}=2.046\,3803$	$C_{34}=-1298.0249$		$\beta_{34}=4.512\,0514$	$C_{34}=5407.1036$

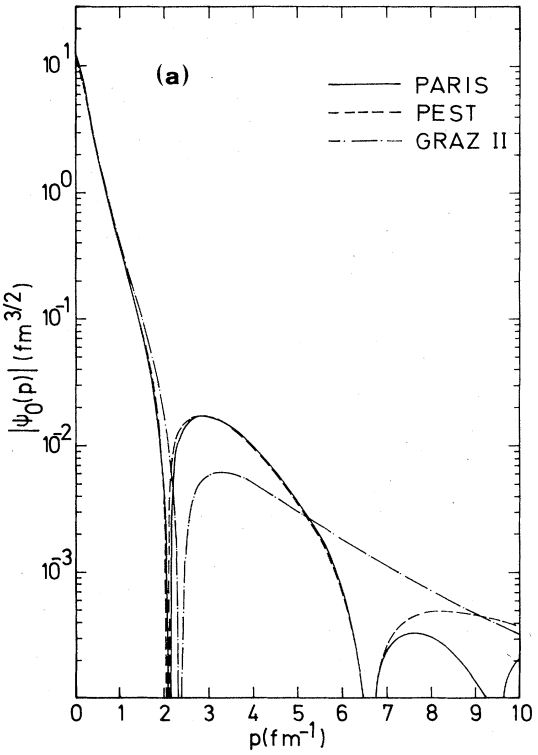

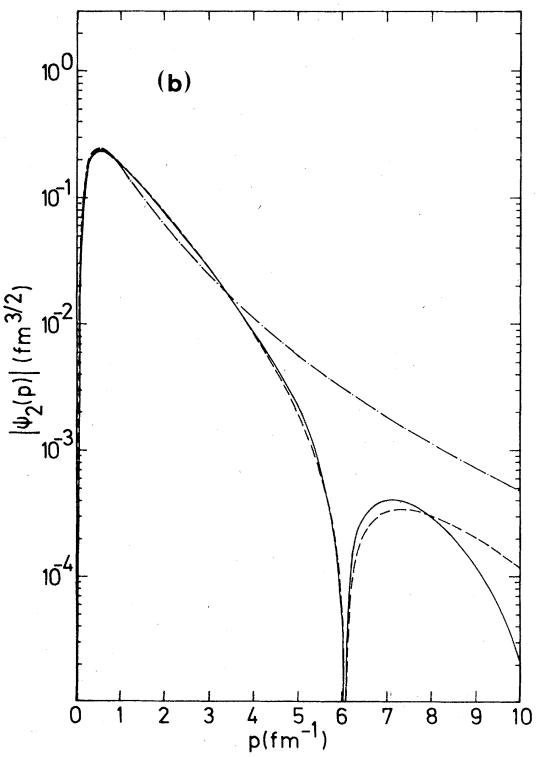

FIG. 12. Momentum-space deuteron wave functions (a) $\psi_0(p)$ and (b) $\psi_2(p)$ for the S and D states, respectively. The results for PEST1 and PEST4 are identical.

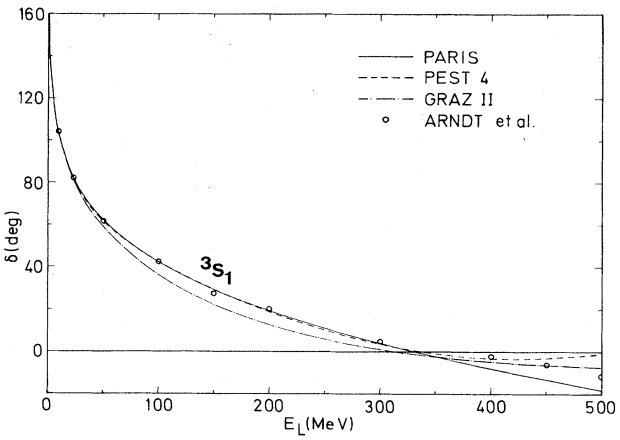

FIG. 13. $^3S_1$ phase shifts.

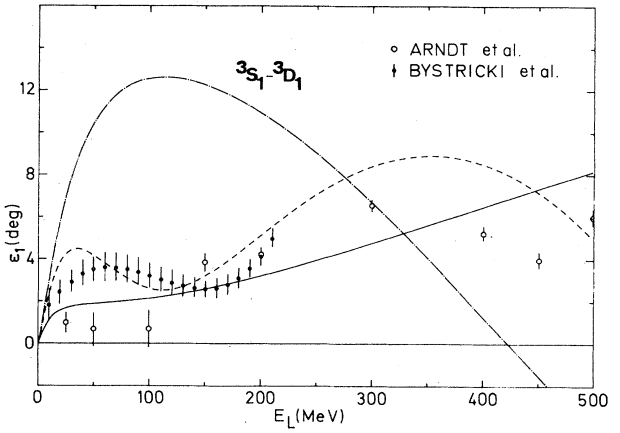

FIG. 14. Mixing parameter ϵ_1. Same description as in Fig. 13.

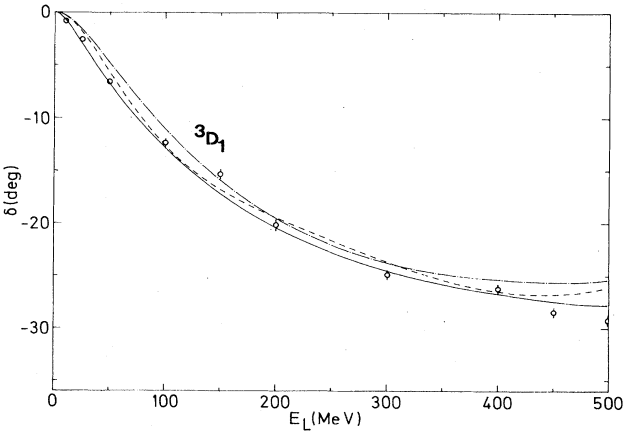

FIG. 15. $^3D_1$ phase shifts. Same description as in Fig. 13.

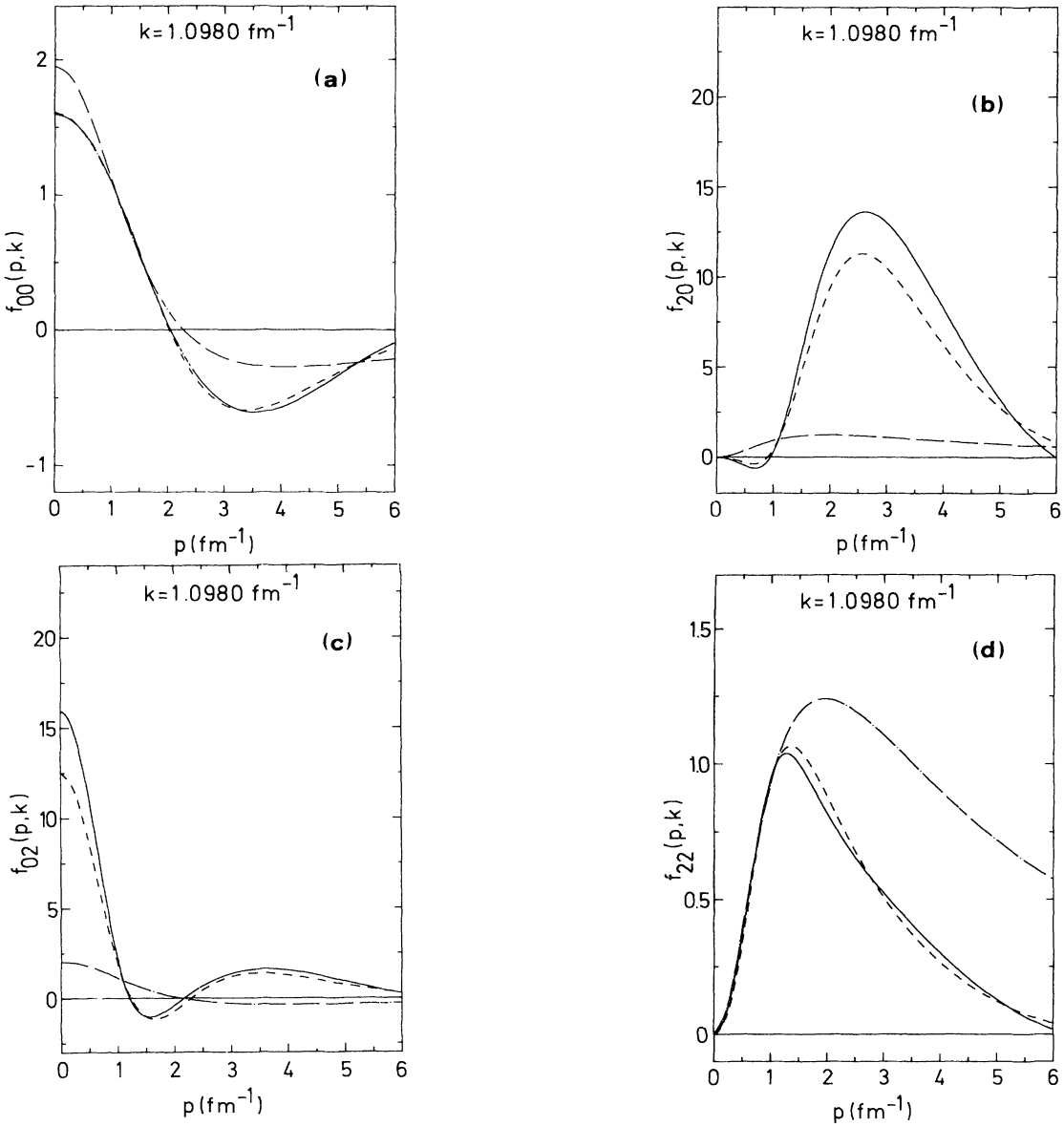

FIG. 16. Half-off-shell functions in $^3S_1$-$^3D_1$ for (a) $^3S_1 \rightarrow {}^3S_1$, (b) $^3S_1 \rightarrow {}^3D_1$, (c) $^3D_1 \rightarrow {}^3S_1$, and (d) $^3D_1 \rightarrow {}^3D_1$ transitions at $E_{\text{lab}} = 100$ MeV. Same description as in Fig. 13.

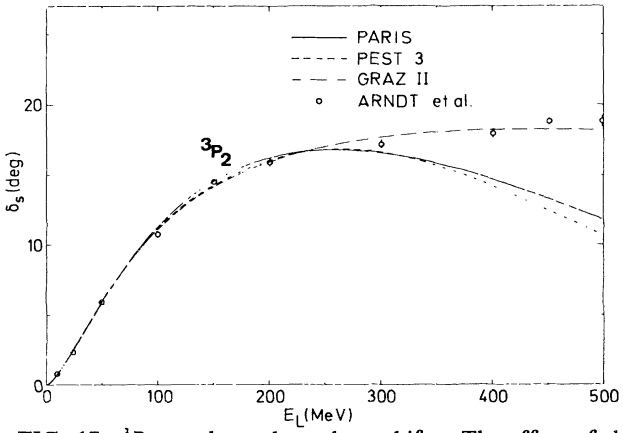

FIG. 17. $^3P_2$ purely nuclear phase shifts. The effect of the Coulomb distortion can be estimated from the figures given in Ref. 6.

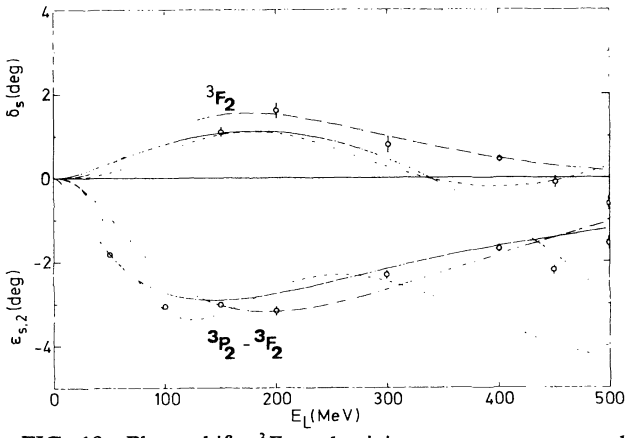

FIG. 18. Phase shifts $^3F_2$ and mixing parameter $\epsilon_{s,2}$ purely nuclear. Same description and remarks as in Fig. 17.

TABLE IX. Parameters of the PEST4 potential in the coupled $^3D_3$-$^3G_3$ partial-wave state.

	β (fm^{-1})	C (fm^0)	λ (MeV fm^{-1})	β (fm^{-1})	C (fm^0)
	$L=2$			$L=4$	
PEST4	$\beta_{11}=1.727\,5071$	$C_{11}=-8.637\,9311$	$\lambda_{11}=-0.098\,992\,244$	$\beta_{11}=2.400\,0943$	$C_{11}=10.076\,418$
	$\beta_{12}=2.549\,3316$	$C_{12}=178.846\,57$	$\lambda_{12}=-0.394\,845\,62$	$\beta_{12}=1.283\,0437$	$C_{12}=-90.394\,797$
	$\beta_{13}=1.911\,1954$	$C_{13}=-114.215\,07$	$\lambda_{13}=0.040\,135\,281$	$\beta_{13}=1.662\,7122$	$C_{13}=283.817\,07$
	$\beta_{14}=4.066\,9172$	$C_{14}=-86.040\,765$	$\lambda_{14}=0.113\,430\,39$	$\beta_{14}=1.558\,1999$	$C_{14}=-204.527\,99$
	$\beta_{21}=1.918\,9644$	$C_{21}=-116.078\,58$	$\lambda_{22}=0.282\,427\,64$	$\beta_{21}=3.919\,4456$	$C_{21}=10.924\,992$
	$\beta_{22}=2.738\,169$	$C_{22}=354.481\,69$	$\lambda_{23}=0.400\,483\,98$	$\beta_{22}=1.571\,9585$	$C_{22}=82.607\,174$
	$\beta_{23}=1.539\,602$	$C_{23}=196.1262$	$\lambda_{24}=-0.346\,772\,41$	$\beta_{23}=1.655\,341$	$C_{23}=-132.302\,66$
	$\beta_{24}=1.915\,9334$	$C_{24}=-419.699\,57$	$\lambda_{33}=-0.142\,241\,21$	$\beta_{24}=2.096\,3683$	$C_{24}=47.770\,331$
	$\beta_{31}=3.227\,718$	$C_{31}=-110.311\,48$	$\lambda_{34}=-0.380\,0097$	$\beta_{31}=4.803\,2746$	$C_{31}=-204.051\,05$
	$\beta_{32}=4.806\,0158$	$C_{32}=483.294\,54$	$\lambda_{44}=0.505\,603\,72$	$\beta_{32}=3.697\,6328$	$C_{32}=-751.6137$
	$\beta_{33}=3.100\,509$	$C_{33}=442.800\,69$	$\lambda_{ij}=\lambda_{ji}$	$\beta_{33}=2.721\,4754$	$C_{33}=1886.8354$
	$\beta_{34}=3.721\,4195$	$C_{34}=-903.639\,57$		$\beta_{34}=1.973\,9909$	$C_{34}=-954.9154$
	$\beta_{41}=2.842\,6813$	$C_{41}=-364.8871$		$\beta_{41}=1.839\,9157$	$C_{41}=-0.242\,991\,33$
	$\beta_{42}=3.354\,9103$	$C_{42}=1848.1193$		$\beta_{42}=2.074\,8484$	$C_{42}=197.5883$
	$\beta_{43}=3.212\,1201$	$C_{43}=2550.6547$		$\beta_{43}=2.283\,176$	$C_{43}=-411.756\,99$
	$\beta_{44}=2.776\,6588$	$C_{44}=-3985.0257$		$\beta_{44}=2.609\,5142$	$C_{44}=229.350\,25$

for coupled channels.[6] A rank-3 PEST parametrization (parameters in Table VIII) was necessary to yield a good on-shell and off-shell approximation to the Paris potential. The phase shifts and the mixing parameter ϵ_2 are shown in Figs. 17 and 18. We laid special emphasis on the reproduction of the lower partial wave, since it should be of greater importance in few-body calculations (cf. the selection of interpolation energies in Table I.) But also the mixing parameter ϵ_2 and the $^3F_2$ phase shift do not deviate more than 1 deg from the Paris prediction up to $E_{\rm lab}\approx 300$ MeV. The half-off-shell functions are evident from Fig. 19 at $E_{\rm lab}=100$ MeV. This point is just between the interpolation energies chosen for this channel (Table I), but still the off-shell approximation to Paris is found to be satisfactory here.

3. $^3D_3$-$^3G_3$

For these coupled partial waves we designed a rank-4 PEST parametrization. No satisfactory approximation was possible with a lower rank. The parameters of the PEST potential are given in Table IX. The on-shell properties are shown in Fig. 20; they exhibit a good agreement with the Paris results. Half-off-shell functions are drawn

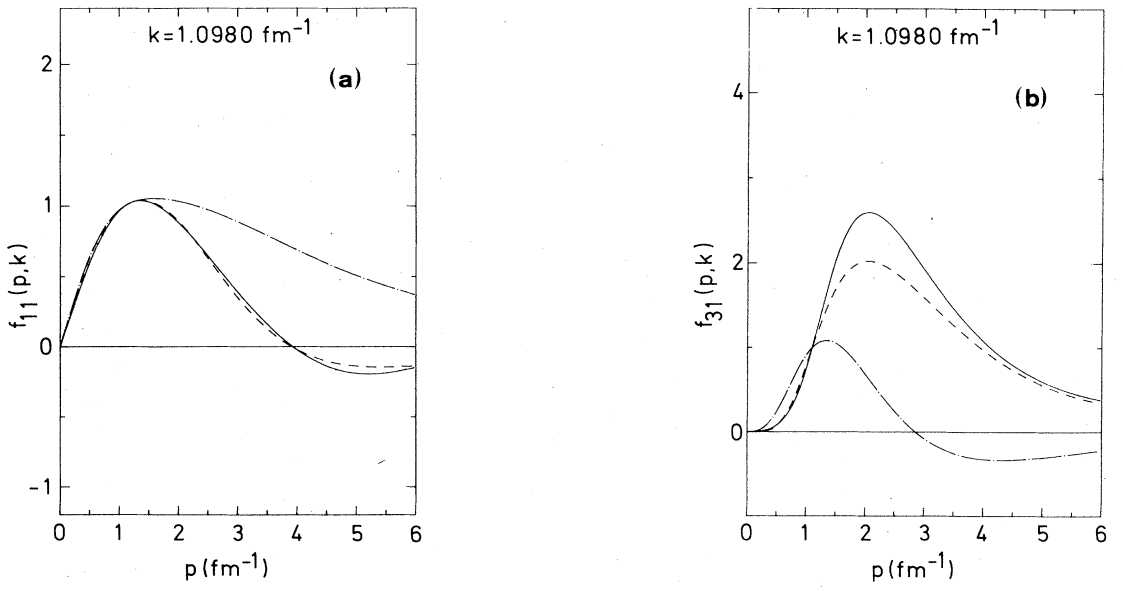

FIG. 19. Half-off-shell functions in $^3P_2$-$^3F_2$ for (a) $^3P_2\rightarrow{}^3P_2$, (b) $^3P_2\rightarrow{}^3F_2$, (c) $^3F_2\rightarrow{}^3P_2$, and (d) $^3F_2\rightarrow{}^3F_2$ transitions at $E_{\rm lab}=100$ MeV. Same description as in Fig. 17.

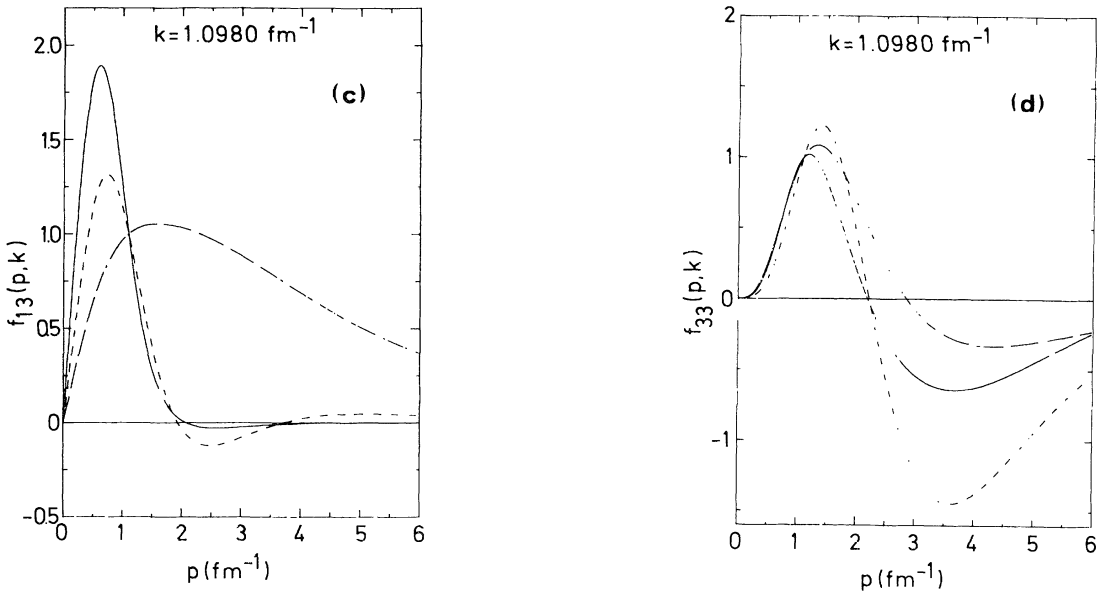

FIG. 19. (*Continued*).

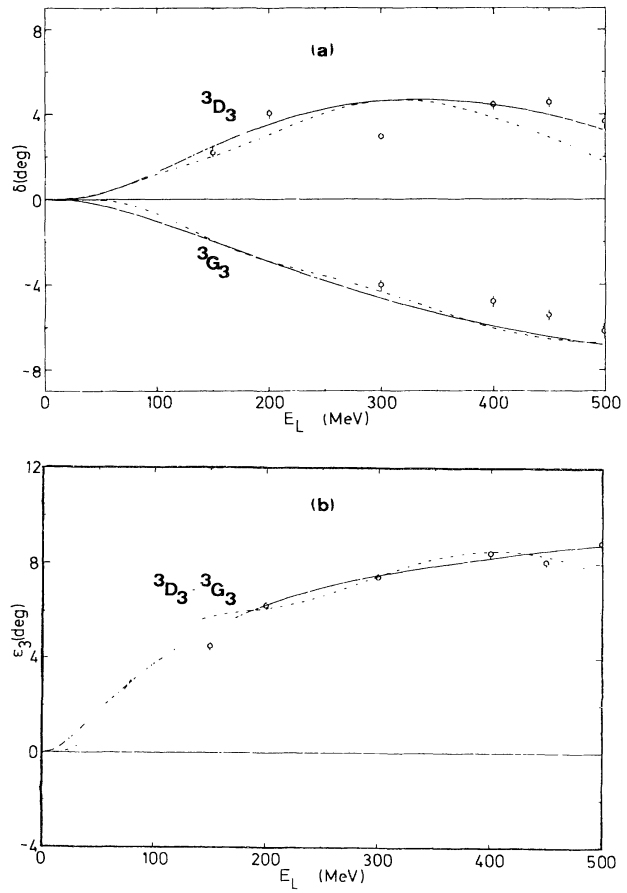

FIG. 20. (a) Phase shifts $^3D_3$ and $^3G_3$ and (b) mixing parameter ϵ_3.

in Fig. 21 again at $E_{\text{lab}}=100$ MeV, i.e., aside the interpolation energy.

IV. DISCUSSION

From the foregoing presentation of the PEST interactions it is clear that these separable representations of the Paris potential incorporate all essential features which are likely to be relevant in various nuclear applications above all in few-body problems. In the following we will shed some light on some of these aspects. Thereby we will also reveal further evidence on the quality of the PEST approximations.

As a first case we consider elastic e-d scattering. It probes on the form of the deuteron wave function and is therefore an important tool to check on potential properties that come through this half-off-shell entity. Since the potentials PEST1 and PEST4 of $^3S_1$-$^3D_1$ both yield practically the same deuteron wave function up to $p \lesssim 6.5$ fm^{-1} (Fig. 12), we found their e-d scattering observables to be indistinguishable from the Paris results over a wide range of momentum transfers, $q^2 \lesssim 40$ fm^{-2}, say. The figures given for the Paris potential by Plessas *et al.*[33] can thus be taken over for the PEST interactions as well. It is clear that they are also in accordance with experimental data, especially for the tensor polarization $p_{zz}(q)$, which has become available only recently[36] (see Fig. 5 of Ref. 33).

Off-shell effects beyond the 2-N bound state enter into N-d scattering, which we have also begun to study using the PEST interactions.[16,27] Because of limitations in the computer code we had available hitherto, we have included just N-N S waves. For some purposes, however, this is already sufficient, namely, for N-d second-order polarizations like spin correlations[16,37] or nucleon-to-nucleon spin transfers[15,27] at low energies. Because of their spin orientations they are mainly governed by N-N S waves and are therefore also fairly sensitive to off-shell effects related to

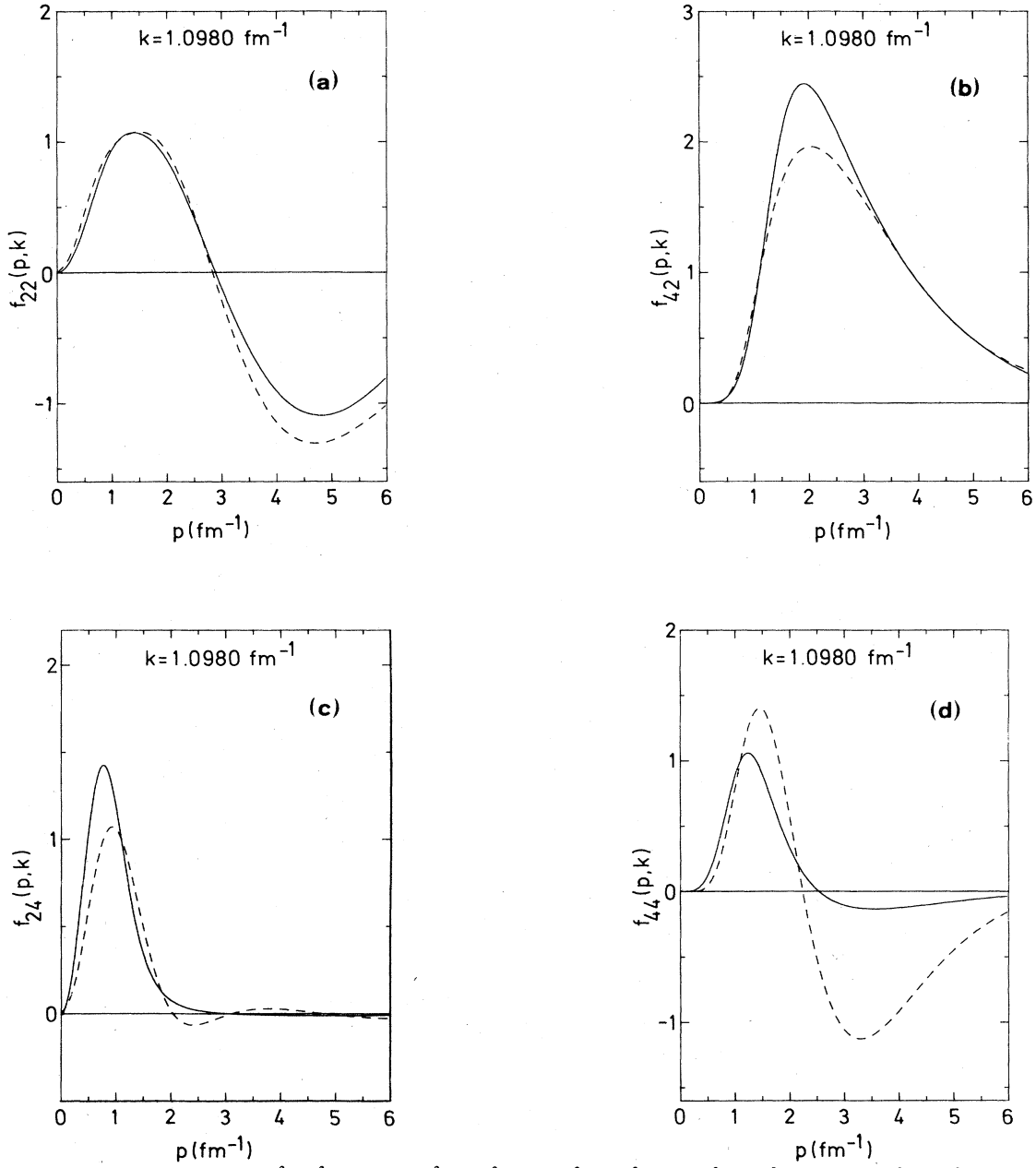

FIG. 21. Half-off-shell functions in $^3D_3$-$^3G_3$ for (a) $^3D_3 \rightarrow {}^3D_3$, (b) $^3D_3 \rightarrow {}^3G_3$, (c) $^3G_3 \rightarrow {}^3D_3$, and (d) $^3G_3 \rightarrow {}^3G_3$ transitions at $E_{\text{lab}} = 100$ MeV. Same description as in Fig. 20.

potential properties at intermediate N-N separations. The reason is that, because of the absence of the centrifugal barrier in S waves, the N-N interaction is tested down to much smaller distances even at low and moderate energies. Accordingly, these regions are more or less hidden to the peripheral interactions in partial waves of higher angular momenta.

As an example for N-d polarization observables we discuss the PEST results for the spin-transfer coefficient $K_y^{y'}$ of the reaction $^2\text{H}(\vec{\text{N}},\vec{\text{N}})^2\text{H}$ at a nucleon incident energy of $E_{\text{N}} = 10$ MeV as studied by Zankel and Plessas.[27] For the (uncharged) n-d case we obtain the solid line in Fig. 22. In order to demonstrate the off-shell sensitivity of this observable we designed—following the method by Zankel *et al.*[16,27]—a Yamaguchi-type potential $Y(E)$ on-shell equivalent to PEST1 but with different off-shell properties. In particular, the $Y(E)$ interaction has a half-off-shell function lacking the zero at $p \approx 2$ fm^{-1} and the adjacent repulsion (for $2 \lesssim p \lesssim 6$ fm^{-1}) as it is present in PEST like in the original Paris potential. For $^1S_0$ this behavior is exemplified in Fig. 23 (the situation in $^3S_1$ is similar). Translated to configuration space (Fig. 24) this means that the Y and PEST interactions differ in the outer attraction ($0.9 \lesssim r \lesssim 1.2$ fm) and in the intermediate-range

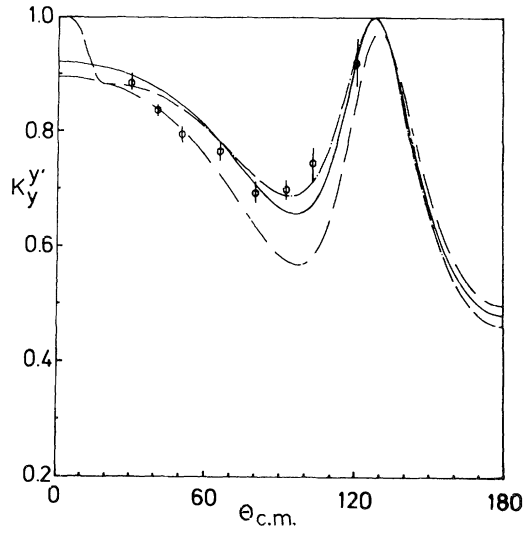

FIG. 22. Spin-transfer coefficient $K_y^{y'}$ of the reaction $^2\mathrm{H}(\vec{\mathrm{N}},\vec{\mathrm{N}})^2\mathrm{H}$ at a nucleon incident energy of $E_N = 10$ MeV. The solid curve is the PEST1 result (only N-N S waves) for neutron-deuteron. The dashed curve belongs to the phase-shift equivalent $Y(E)$ potential. The dashed-dotted curve is the PEST1 prediction for proton-deuteron including approximate Coulomb corrections (Ref. 38). Experimental data are from Sperisen *et al.* (Ref. 15).

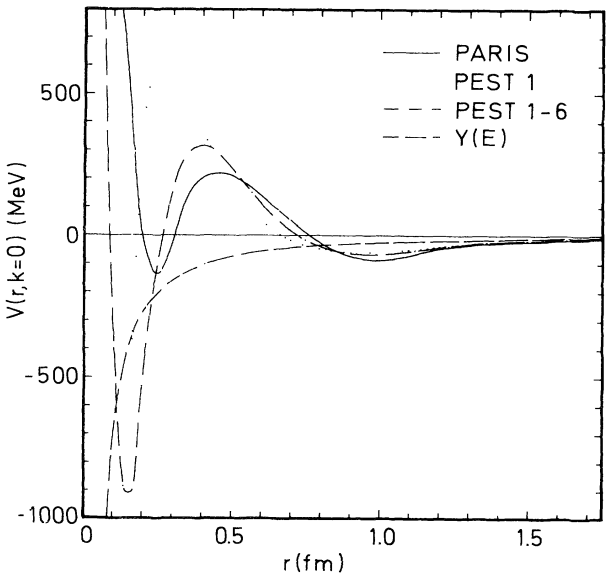

FIG. 24. Configuration-space representations of the potentials at zero momentum in the $^1S_0$ partial wave.

repulsion ($r \lesssim 0.8$ fm). Such features as shown by the Y potential are certainly at variance with meson-exchange theory, which should be reliable in this region; here all meson-theoretical models yield qualitatively the same picture as shown by the Paris potential. We remark, however, that in the long-range domain the Y potential was adapted so as to match one-pion exchange there.[27]

The effect of the off-shell differences of the Yamaguchi-type potential is clearly visible in the spin-transfer coefficient $K_y^{y'}$ (dashed line in Fig. 22). For a comparison with experiment, i.e., p-d data, we must include the Coulomb effects. We add Coulomb-distortion contributions via the method of Haftel and Zankel[38] and thus arrive at the p-d prediction shown for PEST by the dashed-dotted curve in Fig. 22. The result is in fair agreement with experiment, possibly with the exception of forward angles, where the method of Coulomb correction may be less reliable. The Coulomb effects would shift the curve belonging to the Y potential in much the same manner as demonstrated for PEST and thus make its p-d prediction lie aside from phenomenological data. Consequently this observable, like other second-order polarizations, can be useful to preclude N-N interactions with unrealistic off-shell properties.

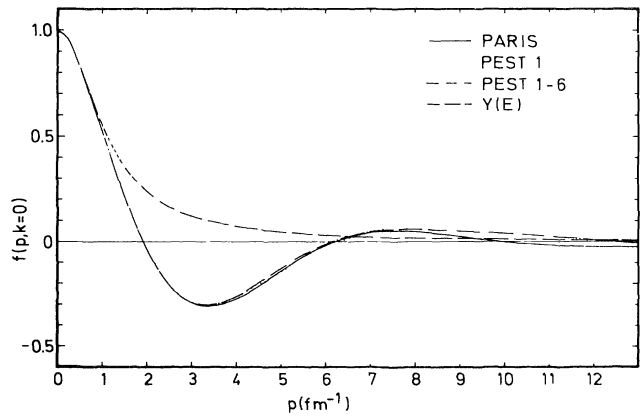

FIG. 23. Half-off-shell functions for $^1S_0$ (p-p) purely nuclear at 2-N threshold.

On the other hand small changes in the off-shell behavior are not visible in such observables. For instance, our PEST1 parametrization presented in Sec. III and the six-term rank-1 interaction (here we denote it by PEST1—6) employed by Zankel *et al.*[16] differ such as is evident from Fig. 23, that is at off-shell momenta $p \gtrsim 7$ fm^{-1}. Translated to configuration space it means that the character of the intermediate-range repulsion is somewhat different but qualitatively the same (at $r \lesssim 0.75$ fm). Such differences, however, have virtually no influence on the reproduction of the N-d polarizations under consideration. In fact, the $K_y^{y'}$ results corresponding to the PEST1 and PEST1—6 interactions would practically be indistinguishable in Fig. 22. From this observation we can also conclude that the deviations that the PEST interactions show from the true Paris potential will have no influence in few-body calculations. The quality of the separable approximations to the Paris potential can therefore be considered of sufficient reliability. As a consequence the result obtained by employing the PEST interactions in various few-body applications furnishes a good estimate of what the Paris potential in its original form would predict. In this connection we would like to add a further

result, which was just lately communicated to us.[26] It concerns the ^{3}H bound-state energy for the PEST interactions; he found it to be $E=-7.30$ MeV with N-N S waves only and $E=-7.35$ MeV including P waves. This should be compared to the results ($E=-7.303$ MeV and $E=-7.384$ MeV, respectively) by Hajduk and Sauer[24] obtained with the original Paris potential via a different (configuration space) calculation. All these first results are very promising and support our hope that the PEST interactions will be of great use for further and more detailed investigations of various few-body systems.

ACKNOWLEDGMENTS

We are grateful to Prof. H. Zingl for encouraging interest in our work and thank our colleagues L. Mathelitsch, W. Schweiger, and H. Zankel for valuable help. The computations were performed at the Rechenzentrum Graz. This work was supported by Fonds zur Förderung der wissenschaftlichen Forschung, Project 4328.

[1]R. A. Arndt, L. D. Roper, R. A. Bryan, R. B. Clark, B. J. VerWest, and P. Signell, Phys. Rev. D **28**, 97 (1983).
[2]J. Bystricki *et al.*, in *Landolt-Börnstein, New Series,* edited by H. Schopper (Springer, Berlin, 1980), Vol. I/9.
[3]D. V. Bugg, Comments Nucl. Part. Phys. (to be published).
[4]W. T. H. van Oers, Comments Nucl. Part. Phys. **10**, 281 (1982).
[5]W. Plessas, L. Mathelitsch, and F. Pauss, Phys. Rev. C **23**, 1340 (1981).
[6]W. Schweiger, W. Plessas, L. P. Kok, and H. van Haeringen, Phys. Rev. C **27**, 515 (1983); **28**, 1414 (1983).
[7]H. W. Fearing, G. R. Goldstein, and M. J. Moravcsik, Phys. Rev. D **29**, 2612 (1984).
[8]See, e.g., the review by A. W. Thomas, in *Few-Body-Systems and Nuclear Forces II,* edited by H. Zingl, M. Haftel, and H. Zankel (Springer, Berlin, 1978).
[9]W. Plessas, Acta Phys. Austriaca **54**, 305 (1982).
[10]M. I. Haftel, L. Mathelitsch, and H. F. K. Zingl, Phys. Rev. C **22**, 1285 (1980).
[11]K. Schwarz, W. Plessas, and L. Mathelitsch, Nuovo Cimento **76A**, 322 (1983).
[12]G. H. Lamot, N. Giraud, and C. Fayard, Nuovo Cimento **57A**, 445 (1980); N. Giraud, C. Fayard, and G. H. Lamot, Phys. Rev. C **21**, 1959 (1980).
[13]M. I. Haftel, Phys. Rev. C **14**, 698 (1976); M. I. Haftel and W. M. Kloet, *ibid.* **15**, 404 (1977).
[14]L. Mathelitsch, W. Plessas, and W. Schweiger, Phys. Rev. C **26**, 65 (1982).
[15]F. Sperisen *et al.*, Phys. Lett. **102B**, 9 (1981); P. Doleschall *et al.*, Nucl. Phys. **A380**, 72 (1982).
[16]H. Zankel, W. Plessas, and J. Haidenbauer, Phys. Rev. C **28**, 538 (1983).
[17]W. Meier and W. Glöckle, Phys. Rev. C **28**, 1807 (1983).
[18]M. Lacombe *et al.*, Phys. Rev. C **21**, 861 (1980).
[19]D. J. Ernst, C. M. Shakin, and R. M. Thaler, Phys. Rev. C **8**, 507 (1973).
[20]J. Haidenbauer, Dissertation, Universität Graz, 1983 (unpublished).
[21]S. C. Pieper, Phys. Rev. C **9**, 883 (1974).
[22]G. W. Bund and H. A. Consoni, Rev. Bras. Fis. **6**, 297 (1976); G. W. Bund and M. C. Tijero, Nuovo Cimento **A57**, 234 (1980).
[23]J. Haidenbauer and W. Plessas, Phys. Rev. C **27**, 63 (1983).
[24]Ch. Hajduk and P. U. Sauer, Nucl. Phys. **A369**, 321 (1981); W. Strueve, Ch. Hajduk, and P. U. Sauer, *ibid.* **A405**, 620 (1983).
[25]E. Hadjimichael, R. Bornais, and B. Goulard, Phys. Rev. Lett. **48**, 583 (1982); E. Hadjimichael, B. Goulard, and R. Bornais, Phys. Rev. C **27**, 831 (1983).
[26]P. Doleschall, private communication; Y. Koike, private communication.
[27]H. Zankel and W. Plessas, Z. Phys. A **317**, 45 (1984).
[28]O. Dumbrajs *et al.*, Nucl. Phys. **B216**, 227 (1983).
[29]P. Doleschall, private communication.
[30]R. Machleidt, private communication.
[31]W. Plessas, L. Streit, and H. Zingl, Acta Phys. Austriaca **40**, 272 (1974).
[32]L. Crepinsek, H. Oberhummer, W. Plessas, and H. Zingl, Acta Phys. Austriaca **39**, 345 (1974); L. Crepinsek, C. B. Lang, H. Oberhummer, W. Plessas, and H. Zingl, *ibid.* **42**, 139 (1975); H. Oberhummer, L. Crepinsek, W. Plessas, and H. F. K. Zingl, *ibid.* **42**, 225 (1975).
[33]W. Plessas, K. Schwarz, and L. Mathelitsch, in *Perspectives in Nuclear Physics at Intermediate Energies,* edited by S. Boffi, C. Ciofi degli Atti, and M. M. Giannini (World Scientific, Singapore, 1984).
[34]R. V. Reid and M. L. Vaida, Phys. Rev. Lett. **34**, 1064 (1975); D. M. Bishop and L. M. Cheung, Phys. Rev. A **20**, 381 (1979).
[35]T. E. O. Ericson, in Proceedings of the 10th International Conference on Few-Body Problems in Physics, Karlsruhe, 1983, Nucl. Phys. **A416**, 281c (1984).
[36]M. E. Schulze *et al.*, Phys. Rev. Lett. **52**, 597 (1984).
[37]R. Schmelzer *et al.*, Phys. Lett. **120B**, 297 (1983).
[38]M. I. Haftel and H. Zankel, Phys. Rev. C **24**, 1322 (1981); H. Zankel and G. M. Hale, *ibid.* **24**, 1384 (1981).